INFLUENCE OF THE MILLING MATERIALS ON THE MECHANOCHEMICAL SYNTHESIS OF MAGNETIC IRON OXIDE NANOPARTICLES

Pedro A. Calderón Bedoya[1], Pablo M. Botta[1], Paula G. Bercoff[2], María A. Fanovich[1]

[1]Instituto de Investigaciones en Ciencia y Tecnología de Materiales, INTEMA (CONICET-UNMdP), Av. Colón 10850, 7600 Mar del Plata, Argentina.
[2] Facultad de Matemática, Astronomía, Física y Computación, FAMAF (UNC), Instituto de Física Enrique Gaviola, IFEG (UNC-CONICET), Medina Allende s/n, Ciudad Universitaria, 5000 Córdoba, Argentina.

ABSTRACT

The aim of this work is to synthesize iron oxide nanoparticles (IONPs) by a mechanochemical process using a high-energy planetary ball mill, with two types of vials and balls (stainless-steel and zirconia) and two reactive mixtures. This preparative route is simple, scalable and environmentally friendly. The influence of milling materials on the structural and magnetic properties of the obtained IONPs was studied. Composition, crystalline structure, morphology and magnetic properties of the IONPs were analyzed by XRD, Raman spectroscopy, SEM, TEM and VSM techniques. An iron oxide with spinel structure, compatible with magnetite (Fe_3O_4) or maghemite (γ-Fe_2O_3), was formed in the prepared samples, when using $FeCl_3$ or $FeCl_3$/Fe with stainless steel vials, or $FeCl_3$/Fe with zirconia vials. The results indicate that the formation of spinel magnetic phases is strongly influenced by the presence of metallic Fe in the starting mixture as well as the nature of the container, which can (or cannot) supply Fe during the milling. The obtained results are presented with a perspective oriented to the biomedical application of the IONPs, considering mean particle sizes, magnetic properties, and chemical stability in simulated body fluids.

Keywords: magnetic nanoparticles, mechanochemistry, magnetite, maghemite

INTRODUCTION

In the last decades, magnetic iron oxide nanoparticles (IONPs) have attracted much attention in biomedical fields such as magnetic resonance imaging, drug delivery, and immobilization of enzymes and proteins [1-10]. Because it is known that proton relaxation times are altered in the presence of induced local magnetic moments, it has recently been proposed that ferrite particles can be used for magnetic resonance imaging (MRI) for diagnostic purposes, for visualizing tumors and metastases in liver, spleen, and lymph nodes, for angiography as a blood pool agent and for visualizing inflammatory lesions like atherosclerotic plaques [11-14]. Magnetite (Fe_3O_4), maghemite (γ-Fe_2O_3) or mixed ferrite nanoparticles have received special attention due to their inherent magnetic properties, but also because the possibility of tailoring their features such as crystalline structure, size, and shape [15-16]. The synthetic production of IONPs can be performed by various methods, such as co-precipitation, solvothermal synthesis, ultrasonic irradiation, laser ablation, chemical reduction, and even plant-based processes [17-26]. Usually, such techniques are often related with high costs, long reaction times, large amounts of waste, and usage of hazardous chemicals, hindering the conversion from lab scale processes to industrial applications. Among those

preparation methods, the mechanochemical synthesis (MS) is an economical and fast method, does not generate toxic residues and allows obtaining nanoparticles of controlled size. Mechanochemical processing allows the production of metal-oxide nanoparticles by means of the high-energy milling of solid precursors, without using organic solvents and/or high temperatures [27]. Also, MS of IONPs enables the development of synthesis processes at large scale [18, 28-29]. The MS method has a direct influence on the degree of crystallinity and point defects concentration in the formed phase. This fact is particularly relevant when the material is manufactured for biomedical purposes since the nanoparticles will be in contact with biological fluids. A high degree of amorphization or many defects in the solid could cause a high degradation of the magnetic phases [14].

Iwasaki *et al*. [28,30] prepared magnetite by a mechanochemical process from ferric hydroxide using stainless-steel pot and balls, without adding a reducing agent. These authors obtained single phase magnetite after 16 h of milling. Its formation was explained based on oxidation–reduction reactions, where the corrosion of iron from the pot and balls played a crucial role. However, the uncontrolled reactivity of the containers and balls can be questionable and possibly lead to not reproducible results at large scale.

A relevant factor in the synthesis of IONPs is the molar ratio of the used reagents. Some authors propose starting from stoichiometric Fe^{2+} and Fe^{3+} ratios, while others use reducing agents to Fe^{3+} precursors. Moreover, the use of clean and eco-friendly reagents spanned a new horizon that includes plant-mediated syntheses, where the active component (plant extract) has a double function: reducing and capping agent [31]. Lin *et al*. studied the mechanochemical synthesis of Fe_3O_4 nanoparticles from a starting mixture of $FeCl_2$ and $FeCl_3$ powders in a 1.2: 2 molar ratio by following the simple processes of ball milling with steel vials and balls, annealing, and washing with water. These authors prepared nanosized Fe_3O_4 powder under an inert atmosphere, obtaining nanoparticles with diameters ranging from 12.5 nm to about 46 nm. However, the influence of the grinding material's chemical nature was not questioned [32]. Carvalho *et al.* reported the preparation of magnetite nanoparticles (12-20 nm) by high-energy ball milling, from stoichiometric amounts of distilled water and metallic iron powder. However, the method required very long treatment times and the obtained magnetite contained 14% metallic iron [33].

In our previous studies, the influence of added Fe powder as reactant during the mechanochemical synthesis of IONPs from three types of solid starting mixtures was comparatively analyzed. The mixture of $FeCl_3.6H_2O$ and NaOH with a 2:6 molar ratio allowed obtaining magnetic NPs (with a mean size of 9 nm) after 12 h of milling, with good stability and no segregation of secondary phases. This fact was associated to the metallic Fe coming from the milling vials and balls, which is detrimental for compositional control. Also, the mixture of $FeCl_2.4H_2O$, $FeCl_3.6H_2O$ and NaOH with a 1:2:8 molar ratio generated a low proportion of magnetic phases at short milling times (2 h), and a high proportion of secondary phases at longer milling times (12 h). On the other hand, the mixture of $FeCl_3.6H_2O$, Fe and NaOH with a 8:1:24 molar ratio proved to be suitable for obtaining magnetic NPs (mean size of 9 nm) after 12 h of milling [29]. These studies showed the need to further investigate the interaction between the reacting system and the container material.

To the best of our knowledge, there are no previous studies that discuss in depth the possible influence of the vials and balls material during the mechanochemical

synthesis of IONPs. For this reason, the aim of this work is to synthesize IONPs through the mechanochemical process using a high-energy planetary ball mill, with two types of vials and balls (stainless steel and zirconia) and two reactive mixtures, as the ones previously studied. The obtained results are presented with an oriented perspective to the IONPs biological application considering mean particle sizes, magnetic properties, and chemical stability in simulated body fluids.

MATERIALS AND METHODS

Ferric chloride hexahydrate ($FeCl_3.6H_2O$, Biopack), Fe powder (Carlo Erba, particle size ~ 1 μm) and sodium hydroxide (NaOH, Anedra) were used as precursors for the synthesis of IONPs. All used chemicals in the experiments were reagents of analytical grade and they were used without further purification. Two precursor mixtures were prepared (10 g per batch), by mixing solid reactants according to optimal conditions previously determined [29]. Table 1 summarizes the selected nomenclature according to the synthesis conditions. Each mixture was mechanochemically treated (MC-treatment) in a planetary ball mill (Fritsch Pulverisette 7), during different times at 1400 rpm. Balls (diameter 10 mm) and vials (25 mL) of stainless-steel (S) and Zirconia (Z) were used as milling materials. Mechanochemical treatments were performed at environmental conditions by using a milling-media/powder-mixture mass ratio of 6.4. After each mechanochemical treatment, the samples were washed with distilled water to eliminate NaCl byproduct; after that, all the samples were dried during 24 h at 50°C.

Table 1: Name and milling conditions of samples obtained by mechanochemical synthesis

Sample	Precursors	Molar ratio	Container and ball material	Milling Time [h]
AS12	$FeCl_3.6H_2O$: NaOH	2 : 6	Stainless Steel	12
AZ12			Zirconia	12
BS12	$FeCl_3.6H_2O$: Fe^0 : NaOH	8 : 1 : 24	Stainless Steel	12
BZ12			Zirconia	12
BZ6			Zirconia	6
BZ3			Zirconia	3

The chemical stability of samples AS12 and BZ12 was evaluated through an immersion assay in simulated body fluid (SBF). The SBF solution was prepared according to ISO 23317 (2014) [34-35]. The volume of SBF to perform the reactivity tests was calculated according to the following equation:

$$V_{SBF} = \frac{Sa}{10} \qquad Eq.\ 1$$

where V_{SBF} is the volume of SBF (mL) and Sa is the apparent surface area of the specimen (mm^2) [36]. Disks of 5 mm in diameter and 1 mm thick were immersed in 2 mL of SBF at 36.5 ºC and kept at a constant temperature for up to 28 days.

Identification of the crystalline phases was carried out by X-ray diffraction (XRD) in a PANalytical diffractometer with Cu-Kα radiation (wavelength λ = 1.54050 Å) at 40 kV and 30 mA. Diffractograms were recorded in a 2θ range between 20º and 70º at a scan rate of 1/min. The mean crystallite size was estimated from the XRD line broadening measurement, using the Scherrer equation [37] for the main peaks, considering the instrument line width.

The lattice parameter *a* was calculated according to *Eq. 2* for cubic systems, averaging interplanar distances (*d*) corresponding to planes (h k l) = (2 2 0), (3 1 1) and (4 4 0):

$$\frac{1}{d^2} = \frac{h^2+k^2+l^2}{a^2} \qquad Eq.\ 2$$

The crystallinity index (CI) was calculated from the XRD patterns by means of the following equation:

$$CI = \frac{A_P}{A_T} .100 \qquad Eq.\ 3$$

where A_P is the area of all crystalline peaks and A_T is the total area (crystalline and amorphous phases) [38]. Also, the CI of a magnetite sample (micrometric particles of concentrate ore) was calculated and taken as a reference. Areas were determined using a commercial data-analysis software.

The Fe^{3+}/Fe^{2+} ratio of the synthesized IONPs was determined using an UV-vis spectrophotometric technique based on the complexation of 1,10-phenanthroline with divalent iron ions. Further details of this quantification methodology can be found in [39].

Raman micro analyses of the obtained powders were performed in a multichannel Renishaw In Via Reflex microspectrometer. Excitation was provided by the 785 nm line of an Ar laser. To enhance the signal-to-noise ratio, 30-50 scans were accumulated, each one having a 15 s exposure to laser power ranging between 30 and 300 mW.

The particle size distributions of the powders were determined by dynamic light scattering (DLS) using a Malvern Zetasizer nano S90 with a 532 nm laser. Powders were dispersed in distilled water (5 mg in 10 mL) and sonicated for 10 min before each measurement.

Transmission electron microscopy (TEM) images of the particles were obtained in a JEOL (JEM-2100) microscope with a voltage of 120 kV. Prior to observation, the samples were suspended in Cu grids after sonicating an isopropanol suspension of the NPs for several minutes. Particle size distributions were obtained from TEM images, counting >200 elements with the Image Pro Plus software.

Magnetization (M) as a function of magnetic field (H) was measured in a vibrating sample magnetometer Lakeshore 7300 (VSM analysis). Hysteresis loops were registered at room temperature applying magnetic fields between of - 13 and +13 kOe. Before performing the measurements, the powders were compacted in 0.5 mm thick pellets of 5 mm diameter.

RESULTS AND DISCUSSION

Fig. 1.a shows XRD patterns of the samples obtained from each reactive mixture in stainless steel and zirconia containers after milling for 12 h, then washed and dried. In every case, single phases are obtained with no traces of secondary phases, within the detection limits of the technique. Peaks belonging to the spinel structure (space group Fd-3m) compatible with magnetite (Fe_3O_4) or maghemite (γ-Fe_2O_3) are observed in the samples except in AZ12, where clear signals of hematite (α-Fe_2O_3) are distinguished. The three most intense peaks for magnetite or maghemite appear around 30.3, 35.5 and 62.9 º 2θ, while those for hematite are 33.1, 35.5 and 53.8 º 2θ, as it can be seen in Figure 1. On the other hand, Fig. 1.b shows the XRD patterns of the samples obtained with reactive system B in zirconia vessels at three different grinding times. All detectable peaks can also be indexed as magnetite or maghemite. From the results, it is concluded that 3 hours of mechanical treatment in zirconia vessels is enough to obtain magnetic iron oxide nanoparticles with the same crystalline structure and purity than the obtained after longer times. The synthesis yield for sample BZ12 was as high as 72%.

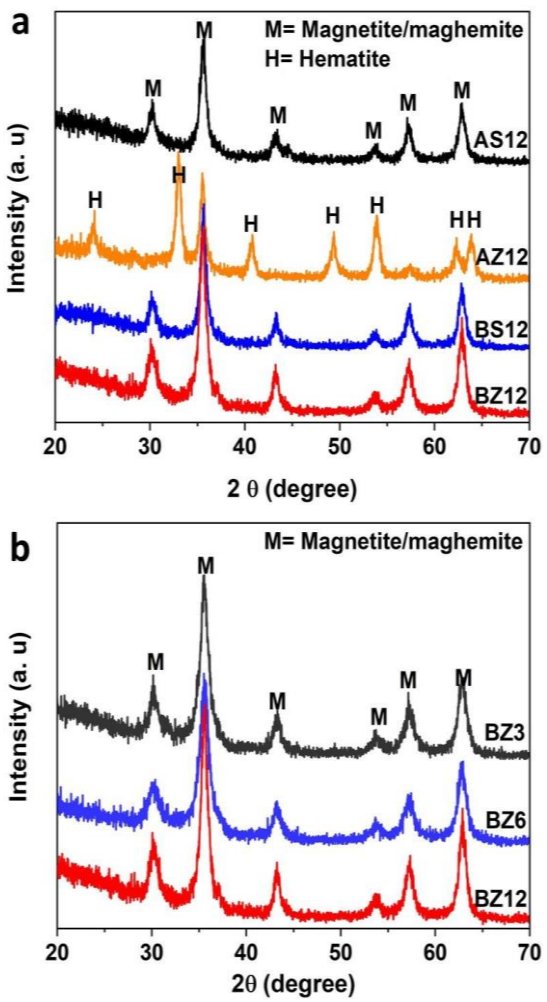

Fig. 1 XRD patterns of **a)** samples A and B obtained by MS in stainless steel and zirconia containers and **b)** B samples obtained in zirconia containers at 3, 6 and 12 h.

The hysteresis loops M(H) of the synthesized samples (Fig. 2) clearly show the influence of the grinding material (zirconia) on sample AZ12, which has very low saturation magnetization, in agreement with the presence of hematite, as detected by XRD. Unlike sample AS12, the powder milled in zirconia vials (AZ12) has not received iron supply (either metallic or Fe^{2+}) from the milling media. The mechanism is based on an oxidation-reduction [30] in which, through a corrosion process, the stainless-steel releases Fe^{2+} ions into the reactive system is essential to obtain magnetic phases by mechanochemical synthesis. The hysteresis loops obtained for the rest of the samples show high magnetization and almost negligible coercivity and remanence, which are features characteristic of small-grained soft ferrites with a superparamagnetic behavior.

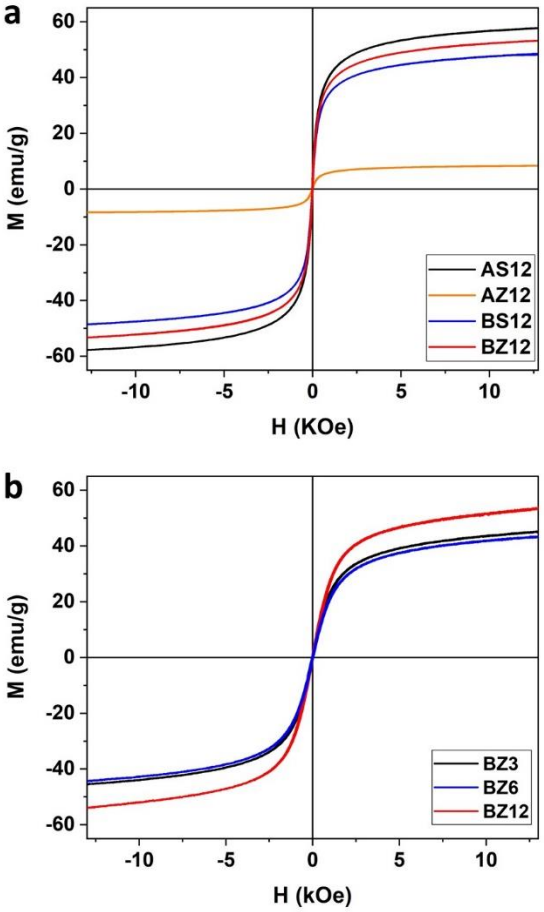

Fig. 2. Magnetization (M) as a function of applied magnetic field (H) for: **a)** samples A and B after milling for 12 h in stainless steel and zirconia containers and **b)** samples obtained in zirconia containers at 3, 6 and 12 h.

Fig. 3 shows the Raman spectra of both series of synthesized samples. Sample AS12 displays the three characteristic bands of maghemite/magnetite, at 365, 511 and 700 cm^{-1} [40-46]. All the bands are very broad and non-symmetric, which could indicate

the coexistence of both spinel phases. This fact agrees with previously published work [47, 48], where similar bands for maghemite/magnetite were found.
Similarly, Raman spectra corresponding to samples BS12 and BZ12 present the three characteristic bands of maghemite and/or magnetite. The Raman spectrum corresponding to sample AZ12 is characteristic of hematite [40-46], being in full agreement with XRD and VSM analyses (Figs. 1 and 2).

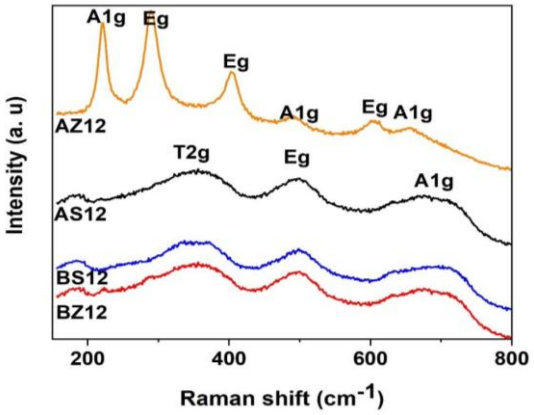

Fig. 3. Raman spectra of samples A and B obtained using stainless steel (S) and zirconia (Z) vials.

To evaluate the physicochemical stability of the obtained IONPs in SBF, magnetic hysteresis loops of $AS12_{SBF}$ and $BZ12_{SBF}$ were measured and are shown in Fig. 4.
The maximum magnetization (Mmax) values reached for both samples are almost identical than those measured for these samples before immersion in SBF (see Fig. 2), which suggests that both samples are physicochemically stable for at least 28 days in SBF.
Likewise, the obtained XRD patterns for these samples confirm that the immersion in the fluid did not change their crystalline structure (see inset in Fig. 4). It is important to mention that the aim of performing the test in SBF was to verify the physicochemical stability of the IONPs under conditions close to the physiological environment to which they could be exposed in a biomedical application.

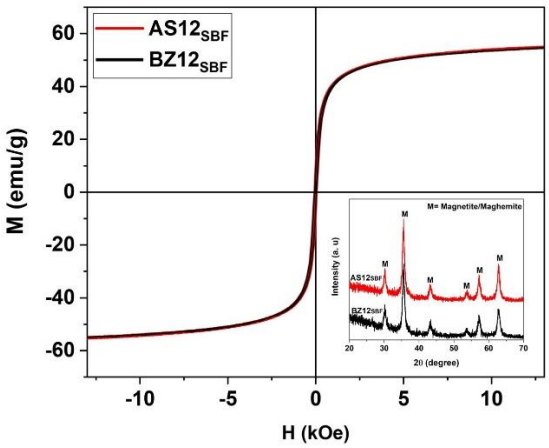

Fig. 4. Magnetization (M) as a function of the applied magnetic field (H) for samples AS12 and BZ12 immersed during 28 days in SBF. The inset shows their corresponding XRD patterns.

Table 2 summarizes the structural, microstructural and magnetic characteristics of each synthesized sample.
Crystallite sizes (determined by the Scherrer equation) range between 10 and 12 nm for all the samples, except for BS12, in which the size is 6 nm. The variation of Mmax (measured at 13 kOe) is consistent with the calculated crystallite sizes, since a system with smaller crystallites has a larger surface area where spin canting occurs, leading to a decrease in the magnetic ordering and thus in Mmax. The smallest crystallite size observed in BS12 could be explained considering that this sample was prepared with the highest metallic Fe content (Fe added as a reactant and Fe provided from the milling media). Therefore, in this solid mixture there are much more reaction points, leading to the formation of a larger number of smaller crystallites.

Table 2: Crystallite size, lattice parameter, crystallinity index ratio (R_{CI}), maximum magnetization Mmax (13kOe) and coercivity Hc values for all the obtained samples. For comparison, typical literature values of some properties for magnetite and maghemite are shown.

Sample	Crystallite size (nm)	Lattice parameter (nm)	R_{CI} (%)	Mmax (13 kOe) (emu/g)	Hc (Oe)
AS12	12	0.83517	74.1	57.8	15
AZ12	-	-	-	5.3	15
BS12	6	0.83477	67.7	48.7	12
BZ12	10	0.83558	65.3	54.9	19
$AS12_{SBF}$	12	0.83559	-	55.9	52
$BZ12_{SBF}$	10	0.83558	-	55.8	48
Magnetite	-	0.83960*	-	92-100 [39]	-
Maghemite	-	0.83515^{+}	-	60-80 [39]	-

*****(PDF 19-0629) $^{+}$(PDF 39-1346)

This fact, in addition to the difficulty of controlling the Fe content incorporated to the reactive mixture, led us to discard the system BS12 for subsequent characterization.

The crystallinity index (CI) is a quantitative indicator of crystallinity and in XRD is defined as the volume fraction of a phase's crystalline proportion in each sample; CI represents the average size, perfection and arrangement of crystallites [49]. CI calculated for samples AS12, BS12 and BZ12 were 46.6, 42.6 and 41.1, respectively. Table 2 reports the values of CI ratios R_{CI} for the three samples, being R_{CI} the corresponding CI relative to the magnetite reference. The obtained R_{CI} values are higher than 65% in every case, indicating that the IONPs are quite crystalline, considering the very small crystallite sizes.

The lowest value for maximum magnetization (5.3 emu/g) was attained in sample AZ12, which is consistent with its phase composition, mainly paramagnetic hematite. Eventually, this synthesis route could be an interesting option for obtaining hematite nanoparticles, although it was not the purpose of the present work.

All samples, except BS12, display magnetization values of the same order of magnitude (54-57 emu/g), being close to those reported for magnetic nanoparticles obtained by different synthesis methods (see **Table 3**).

Coercivity values for most of the samples are in the expected range for nanometric soft magnetic nanoparticles (lower than 20 Oe). Samples immersed in SBF exhibit an increase of Hc, probably due to physicochemical phenomena produced on the nanoparticles surface (such as ions adsorption, effects of dissolution-precipitation, etc.). Immersion of samples in SBF did not produce other effects on the properties registered in Table 2, demonstrating the chemical and structural stability of the synthesized IONPs.

In every sample, the lattice parameter is closer to maghemite than magnetite, despite the great structural similitude between both spinels. The Fe^{3+}/Fe^{2+} ratio calculated from the spectrophotometric determination gave 4.2 for sample BZ12, corresponding to a

composition of 19 wt.% magnetite and 81 wt.% maghemite.

According to the results obtained so far, only the microstructural characterization of samples AS12, BS12 and BZ12 will be presented.

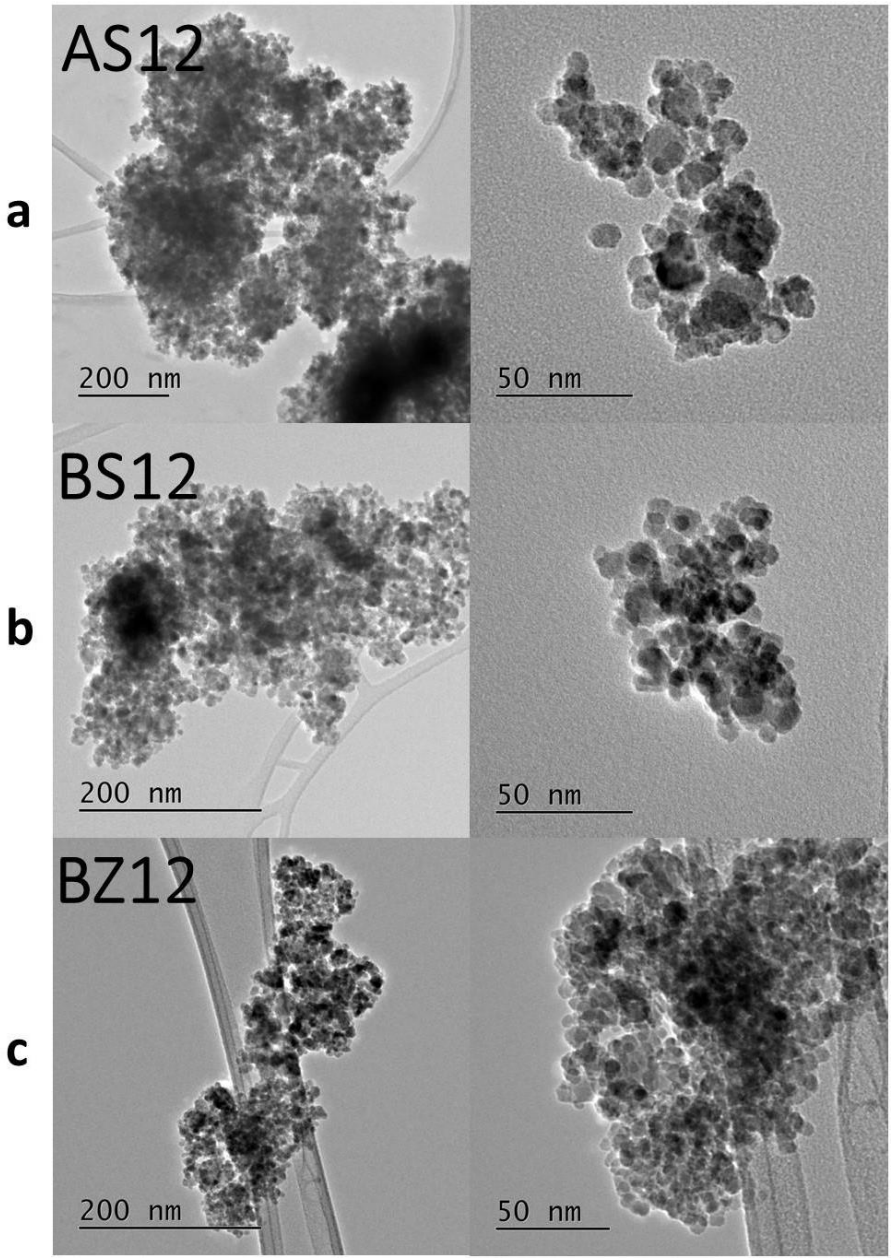

Fig. 5. TEM images of samples prepared with precursor A in steel vials (a) and with precursor B (both in steel (b) and zirconia (c) vials) obtained after 12 h of milling.

TEM images of samples AS12, BS12 and BZ12 are shown in Fig. 5. In every case, agglomerates of particles with quasi-spherical morphology are observed. The nanoparticles have an average size between 6 and 12 nm, which agrees with the crystallite size calculated using the Scherrer equation (Table 2).

Table 3 summarizes previously reported data of saturation magnetization (Ms) and particle size of IONPs synthesized by different methods. There is not a clear correlation between magnetization and nanoparticle size, which indicates that besides particle size, there are many variables that affect the magnetic behavior of the IONPs, such as crystallinity, particle morphology, agglomeration, adsorption effects, particle interactions, nature of the precursors, synthesis conditions, etc. In this context, IONPs obtained in this investigation exhibit very good magnetic properties, considering their average size, probably due to a relatively high crystallinity degree. Some advantages of the used mechanochemical synthesis are the reproducibility, scalability and the absence of organic solvents (toxic and/or expensive). Also, the obtained particle size distributions are quite narrow. On the other hand, the IONPs prepared by MS have a great tendency to agglomerate. Moreover, mechanical energy can induce structural crystalline damage during the process. These aspects represent the drawbacks and limitations of this synthesis method.

Table 3 Summary of some methods for obtaining nanoparticles with their respective saturation magnetization values

Synthesis method	Particle size (nm)	Saturation magnetization (emu/g)	Reference
Coprecipitation	6 12	37.50 60.57	[50]
	7-10	64 75	[51]
	30	80	[6]
	10	28	[52]
	10	53	[53]
Coprecipitation- sonochemical probe	11	65.35	[54]
Solution combustion (heating mantle)	20	66.6	[55]
Solution combustion (microwave)	15	41.8	
Solvothermal synthesis	5.1 14.3	9.3 31.3	[56]
Solvothermal	45	60	[57]
Magnetic nanocatalyst	30 7 20 30	84 72 75 81	[58, 59]
One-step solution auto-combustion process	50 80	7.33 5.66	[60]
Sol-gel	120 100	2.69 3.67	
Electric discharge method	10.3-35.5	53.97-65.01	[61]
Mechanochemical	8.8-10.9	75.2-62.6	[18]

Figure 6 shows a graphical scheme representing the mechanism proposed by the solid-state reaction occurring during the mechanochemical activation, either performed with stainless-steel or zirconia milling media. In both cases, metallic iron is a necessary reactant to produce IONPs with high magnetization, since this element acts as a reducing agent, forming Fe^{2+} cations. In system A, metallic Fe comes from the vials and balls, whereas in system B the metal is one of the starting materials. The reaction of Fe^{2+} with the ferric precursor (Fe^{3+}) in a basic media leads to the formation of Fe_3O_4 (magnetite), which can be totally or partially oxidized to γ-Fe_2O_3 (maghemite). Despite this oxide has only ferric cations in the structure, its formation comes from magnetite, as an intermediary phase, as it has been reported in other synthesis methods [61-64]. This fact could be explained considering the same cubic spinel structure of both oxides, in contrast with hematite (rhombohedral).

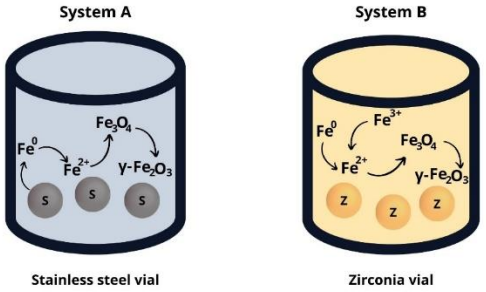

Fig 6. Graphical scheme symbolizing the sequence of mechanochemical reactions in both systems.

Conclusion

Magnetic IONPs with sizes between 6 and 12 nm could be prepared from mechanochemical treatment of solid iron precursors and NaOH. The synthesized nanoparticles are composed by a mixture of magnetite and maghemite. Magnetic properties at room temperature showed the expected behavior for this kind of systems: high saturation magnetization (55-57 emu/g) and very low coercivity (12-19 Oe). The measured values are in the order of magnitude reported for IONPs prepared by other methods, such as coprecipitation and sol-gel.

The chemical nature of the vials and balls used during the milling strongly influences the formed iron oxide phases. The metallic iron supplied by the stainless-steel milling media is essential to the formation of magnetite/maghemite nanoparticles. The use of zirconia vials and balls requires the addition of metallic iron to the reactive mixture to obtain the ferrimagnetic IONPs, otherwise hematite forms. This fact demonstrates that metallic iron has to be present in the reactive system to obtain magnetite/maghemite nanoparticles. The mechanosynthesis performed with zirconia milling media is the preferred route because it allows a better control of the metallic iron added to the reactive mixture.

Immersion in SBF for 28 days did not produce physicochemical alterations of the IONPs, which kept the same crystalline structure and magnetic properties, making these IONPs suitable for biomedical applications.

CRediT authorship contribution statement

Pedro A. Calderon Bedoya: Methodology, Formal analysis, Investigation, Writing - original draft, Visualization. Pablo M. Botta: Conceptualization, Methodology, Formal analysis, Investigation, Resources, Writing - original draft, Writing - review & editing, Supervision. Paula G. Bercoff: Formal analysis, Investigation, Resources, Writing - original draft, Writing - review & editing. María A. Fanovich: Conceptualization, Methodology, Formal analysis, Investigation, Resources, Writing - original draft, Writing - review & editing, Supervision, Project administration.

Declaration of competing interest

The authors declare that they have no known competing financial interests or personal relationships that could have appeared to influence the work reported in this paper.

Acknowledgements

The authors gratefully acknowledge CONICET, Universidad Nacional de Córdoba and Universidad Nacional de Mar del Plata for the financial support given to this work.

References

[1] D. M. Neto *et al.*, «A novel amino phosphonate-coated magnetic nanoparticle as MRI contrast agent», *Applied Surface Science*, vol. 543, p. 148824, 2021.

[2] S. Arsalani *et al.*, «Magnetic Fe3O4 nanoparticles coated by natural rubber latex as MRI contrast agent», *Journal of Magnetism and Magnetic Materials*, vol. 475, pp. 458-464, 2019.

[3] C. Oka, K. Ushimaru, N. Horiishi, T. Tsuge, y Y. Kitamoto, «Core–shell composite particles composed of biodegradable polymer particles and magnetic iron oxide nanoparticles for targeted drug delivery», *Journal of Magnetism and Magnetic Materials*, vol. 381, pp. 278-284, 2015.

[4] S. Ayyanaar *et al.*, «Iron oxide nanoparticle core-shell magnetic microspheres: Applications toward targeted drug delivery», *Nanomedicine: Nanotechnology, Biology and Medicine*, vol. 24, p. 102134, 2020.

[5] A. Marcu *et al.*, «Magnetic iron oxide nanoparticles as drug delivery system in breast cancer», *Applied Surface Science*, vol. 281, pp. 60-65, 2013.

[6] M. Ebadi, K. Buskaran, S. Bullo, M. Z. Hussein, S. Fakurazi, y G. Pastorin, «Drug delivery system based on magnetic iron oxide nanoparticles coated with (polyvinyl alcohol-zinc/aluminium-layered double hydroxide-sorafenib)», *Alexandria Engineering Journal*, vol. 60, n.º 1, pp. 733-747, feb. 2021, doi: 10.1016/j.aej.2020.09.061.

[7] W. R. Glomm *et al.*, «Immobilized protease on magnetic particles for enzymatic protein hydrolysis of poultry by-products», *LWT*, vol. 152, p. 112327, 2021.

[8] S. S. Patil y V. K. Rathod, «Combined effect of enzyme co-immobilized magnetic nanoparticles (MNPs) and ultrasound for effective extraction and purification of curcuminoids from Curcuma longa», *Industrial Crops and Products*, vol. 177, p. 114385, 2022.

[9] I. A. T. Ximenes, P. C. O. de Oliveira, C. A. Wegermann, y M. C. de Moraes, «Magnetic particles for enzyme immobilization: A versatile support for ligand screening», *Journal of Pharmaceutical and Biomedical Analysis*, vol. 204, p. 114286, 2021.

[10] H. E. Andrada, L. Venosta, S. E. Jacobo, O. Fernando Silva, R. Darío Falcone, y P. G. Bercoff, «Highly Stable Nanostructured Magnetic Vesicles as Doxorubicin Carriers for Field-assisted Therapies», *ChemNanoMat*, vol. 8, n.º 4, p. e202100409, 2022.

[11] C. Corot, P. Robert, J.-M. Idée, y M. Port, «Recent advances in iron oxide nanocrystal technology for medical imaging», *Advanced drug delivery reviews*, vol. 58, n.º 14, pp. 1471-1504, 2006.

[12] M. Russell y Y. Anzai, «Ultrasmall superparamagnetic iron oxide enhanced MR imaging for lymph node metastases», *Radiography*, vol. 13, pp. e73-e84, 2007.

[13] S. M. Dadfar *et al.*, «Iron oxide nanoparticles: Diagnostic, therapeutic and theranostic applications», *Advanced drug delivery reviews*, vol. 138, pp. 302-325, 2019.

[14] J. W. Bulte, «Superparamagnetic iron oxides as MPI tracers: A primer and review of early applications», *Advanced drug delivery reviews*, vol. 138, pp. 293-301, 2019.

[15] A. G. Roca, L. Gutiérrez, H. Gavilán, M. E. F. Brollo, S. Veintemillas-Verdaguer, y M. del Puerto Morales, «Design strategies for shape-controlled magnetic iron oxide nanoparticles», *Advanced drug delivery reviews*, vol. 138, pp. 68-104, 2019.

[16] C. Song, W. Sun, Y. Xiao, y X. Shi, «Ultrasmall iron oxide nanoparticles: Synthesis, surface modification, assembly,

and biomedical applications», *Drug Discovery Today*, vol. 24, n.º 3, pp. 835-844, 2019.

[17] F. E. Echeverría y J. C. Acuña, «Síntesis de óxidos de hierro nanoparticulados.», *Scientia et technica*, vol. 4, n.º 36, pp. 993-998, 2007.

[18] T. Iwasaki, K. Kosaka, T. Yabuuchi, S. Watano, T. Yanagida, y T. Kawai, «Novel mechanochemical process for synthesis of magnetite nanoparticles using coprecipitation method», *Advanced Powder Technology*, vol. 20, n.º 6, pp. 521-528, nov. 2009, doi: 10.1016/j.apt.2009.06.002.

[19] J. Li, S. Wang, X. Shi, y M. Shen, «Aqueous-phase synthesis of iron oxide nanoparticles and composites for cancer diagnosis and therapy», *Advances in Colloid and Interface Science*, vol. 249, pp. 374-385, nov. 2017, doi: 10.1016/j.cis.2017.02.009.

[20] X. L. Liu y H. M. Fan, «Innovative magnetic nanoparticle platform for magnetic resonance imaging and magnetic fluid hyperthermia applications», *Current Opinion in Chemical Engineering*, vol. 4, pp. 38-46, 2014, doi: 10.1016/j.coche.2013.12.010.

[21] G. Ren, L. Yang, Z. Zhang, B. Zhong, X. Yang, y X. Wang, «A new green synthesis of porous magnetite nanoparticles from waste ferrous sulfate by solid-phase reduction reaction», *Journal of Alloys and Compounds*, vol. 710, pp. 875-879, 2017, doi: 10.1016/j.jallcom.2017.03.337.

[22] E. Nourafkan, M. Asachi, H. Gao, G. Raza, y D. Wen, «Synthesis of stable iron oxide nanoparticle dispersions in high ionic media», *Journal of Industrial and Engineering Chemistry*, vol. 50, pp. 57-71, jun. 2017, doi: 10.1016/j.jiec.2017.01.026.

[23] B. K. Sodipo y A. A. Aziz, «Recent advances in synthesis and surface modification of superparamagnetic iron oxide nanoparticles with silica», *Journal of Magnetism and Magnetic Materials*, vol. 416, pp. 275-291, oct. 2016, doi: 10.1016/j.jmmm.2016.05.019.

[24] V. A. Svetlichnyi, A. V. Shabalina, I. N. Lapin, D. A. Goncharova, D. A. Velikanov, y A. E. Sokolov, «Study of iron oxide magnetic nanoparticles obtained via pulsed laser ablation of iron in air», *Applied Surface Science*, vol. 462, pp. 226-236, 2018.

[25] S. D. Roy, K. C. Das, y S. S. Dhar, «Conventional to green synthesis of magnetic iron oxide nanoparticles; its application as catalyst, photocatalyst and toxicity: A short review», *Inorganic Chemistry Communications*, vol. 134, dic. 2021, doi: 10.1016/j.inoche.2021.109050.

[26] Y. Xia *et al.*, «Iron oxide nanoparticles in liquid or powder form enhanced osteogenesis via stem cells on injectable calcium phosphate scaffold», *Nanomedicine: Nanotechnology, Biology, and Medicine*, vol. 21, oct. 2019, doi: 10.1016/j.nano.2019.102069.

[27] T. Tsuzuki, «Mechanochemical synthesis of metal oxide nanoparticles», *Communications Chemistry*, vol. 4, n.º 1, pp. 1-11, 2021.

[28] T. Iwasaki, N. Sato, K. Kosaka, S. Watano, T. Yanagida, y T. Kawai, «Direct transformation from goethite to magnetite nanoparticles by mechanochemical reduction», *Journal of Alloys and Compounds*, vol. 509, n.º 4, ene. 2011, doi: 10.1016/j.jallcom.2010.10.029.

[29] P. A. Calderón Bedoya, P. M. Botta, P. G. Bercoff, y M. A. Fanovich, «Magnetic iron oxides nanoparticles obtained by mechanochemical reactions from different solid precursors», *Journal of Alloys and Compounds*, vol. 860, 2021, doi: 10.1016/j.jallcom.2020.157892.

[30] T. Iwasaki, N. Sato, H. Nakamura, y S. Watano, «An experimental investigation of aqueous-phase synthesis of magnetite nanoparticles via mechanochemical reduction of goethite», en *Advanced Powder Technology*, mar. 2013, vol. 24, n.º 2, pp. 482-486. doi: 10.1016/j.apt.2012.11.014.

[31] Y. C. López y M. Antuch, «Morphology control in the plant-mediated synthesis of magnetite nanoparticles», *Current Opinion in Green and Sustainable Chemistry*, vol. 24, pp. 32-37, ago. 2020, doi: 10.1016/j.cogsc.2020.02.001.

[32] C. R. Lin, Y. M. Chu, y S. C. Wang, «Magnetic properties of magnetite nanoparticles prepared by mechanochemical reaction», *Materials Letters*, vol. 60, n.º 4, pp. 447-450, feb. 2006, doi: 10.1016/J.MATLET.2005.09.009.

[33] J. F. D. Carvalho, S. N. D. Medeiros, M. A. Morales, A. L. Dantas, y A. S. Carriço, «Synthesis of magnetite nanoparticles by high

energy ball milling», en *Applied Surface Science*, jun. 2013, vol. 275, pp. 84-87. doi: 10.1016/j.apsusc.2013.01.118.

[34] «Implants for surgery-In vitro evaluation for apatite-forming ability of implant materials COPYRIGHT PROTECTED DOCUMENT», 2014. [En línea]. Disponible en: www.sis.se.Buytheentirestandardviahttps://www.sis.se/std-917469Webwww.iso.orgThispreviewisdownloadedfromwww.sis.se.Buytheentirestandardviahttps://www.sis.se/std-917469

[35] T. Kokubo y H. Takadama, «How useful is SBF in predicting in vivo bone bioactivity?», *Biomaterials*, vol. 27, n.º 15, pp. 2907-2915, 2006, doi: 10.1016/j.biomaterials.2006.01.017.

[36] D. Rohanová, D. Horkavcová, A. Helebrant, y A. R. Boccaccini, «Assessment of in vitro testing approaches for bioactive inorganic materials», *Journal of Non-Crystalline Solids*, vol. 432, pp. 53-59, ene. 2016, doi: 10.1016/j.jnoncrysol.2015.03.016.

[37] B. D. Cullity, *Elements of X-ray Diffraction*. Addison-Wesley Publishing, 1956.

[38] V. Pecharsky y P. Zavalij, «Fundamentals of Powder Diffraction and Structural Characterization of Materials (2nd Version)», 2009.

[39] J. Changzhao, Y. Siyu, G. Neng, P. Hongchun, L. Hong, «A method for determination of $[Fe^{3+}]/[Fe^{2+}]$ ratio in superparamagnetic iron oxide, Journal of Magnetism and Magnetic Materials 439 (2017) 126–134. doi:10.1016/j.jmmm.2017.04.073.

[40] R. M. Cornell y U. Schwertmann, The Iron Oxides. Wiley, 2003. doi: 10.1002/3527602097.

[41] C. Markovski *et al.*, «Abiotic versus biotic iron mineral transformation studied by a miniaturized backscattering Mössbauer spectrometer (MIMOS II), X-ray diffraction and Raman spectroscopy», *Icarus*, vol. 296, pp. 49-58, nov. 2017, doi: 10.1016/j.icarus.2017.05.017.

[42] C. J. Letti, L. G. Paterno, M. A. Pereira-da-Silva, P. C. Morais, y M. A. G. Soler, «The role of polymer films on the oxidation of magnetite nanoparticles», *Journal of Solid State Chemistry*, vol. 246, pp. 57-64, feb. 2017, doi: 10.1016/j.jssc.2016.10.027.

[43] I. Martínez-Mera, C. Gutiérrez-Wing, C. Argánis-Juárez, y A. R. Vilchis-Nestor, «Reduction of maghemite to magnetite over 304SS, in the presence of silver nanoparticles», *Surface and Coatings Technology*, vol. 324, pp. 338-344, sep. 2017, doi: 10.1016/j.surfcoat.2017.05.079.

[44] L. Slavov *et al.*, «Raman spectroscopy investigation of magnetite nanoparticles in ferrofluids», *Journal of Magnetism and Magnetic Materials*, vol. 322, n.º 14, pp. 1904-1911, jul. 2010, doi: 10.1016/j.jmmm.2010.01.005.

[45] M. Krajewski *et al.*, «Impact of thermal oxidation on chemical composition and magnetic properties of iron nanoparticles», *Journal of Magnetism and Magnetic Materials*, vol. 458, pp. 346-354, jul. 2018, doi: 10.1016/j.jmmm.2018.03.047.

[46] M. Bajt Leban y T. Kosec, «Characterization of corrosion products formed on mild steel in deoxygenated water by Raman spectroscopy and energy dispersive X-ray spectrometry», *Engineering Failure Analysis*, vol. 79, pp. 940-950, sep. 2017, doi: 10.1016/j.engfailanal.2017.03.022.

[47] D. V. de Sousa, J. C. Ker, C. E. R. Schaefer, M. J. Rodet, L. M. Guimarães, y J. F. Felix, «Magnetite originating from bonfires in a Brazilian prehistoric Anthrosol: A micro-Raman approach», *CATENA*, vol. 171, pp. 552-564, dic. 2018, doi: 10.1016/j.catena.2018.07.036.

[48] M. E. Mejia-Santillan *et al.*, «Physical and arsenic adsorption properties of maghemite and magnetite sub-microparticles», *Journal of Magnetism and Magnetic Materials*, vol. 451, pp. 594-601, abr. 2018, doi: 10.1016/j.jmmm.2017.11.111.

[49] Y. Sa *et al.*, «Are different crystallinity-index-calculating methods of hydroxyapatite efficient and consistent?», *New Journal of Chemistry*, vol. 41, n.º 13, pp. 5723-5731, 2017.

[50] Y. Zhu y Q. Wu, «Synthesis of magnetite nanoparticles by precipitation with forced mixing», 1999.

[51] A. Omelyanchik *et al.*, «Iron oxide nanoparticles synthesized by a glycine-modified coprecipitation method: Structure and magnetic properties», *Colloids and*

Surfaces A: Physicochemical and Engineering Aspects, vol. 647, p. 129090, ago. 2022, doi: 10.1016/j.colsurfa.2022.129090.

[52] A. Lazzarini *et al.*, «Investigation of physico-chemical and catalytic properties of the coating layer of silica-coated iron oxide magnetic nanoparticles», *Journal of Physics and Chemistry of Solids*, vol. 153, jun. 2021, doi: 10.1016/j.jpcs.2021.110003.

[53] B. Shaabani, H. Maleki, y J. Rakhtshah, «Environmentally benign synthesis of pyranopyrazole derivatives by cobalt Schiff-base complexes immobilized on magnetic iron oxide nanoparticles», *Journal of Organometallic Chemistry*, vol. 897, pp. 139-147, oct. 2019, doi: 10.1016/j.jorganchem.2019.06.030.

[54] C. H. Pérez-Beltrán *et al.*, «One-minute and green synthesis of magnetic iron oxide nanoparticles assisted by design of experiments and high energy ultrasound: Application to biosensing and immunoprecipitation», *Materials Science and Engineering C*, vol. 123, abr. 2021, doi: 10.1016/j.msec.2021.112023.

[55] A. Căpraru, E. A. Moacă, C. Păcurariu, R. Ianoș, R. Lazău, y L. Barbu-Tudoran, «Development and characterization of magnetic iron oxide nanoparticles using microwave for the combustion reaction ignition, as possible candidates for biomedical applications», *Powder Technology*, vol. 394, pp. 1026-1038, dic. 2021, doi: 10.1016/j.powtec.2021.08.093.

[56] X. Zuo, H. Ding, J. Zhang, T. Fang, y D. Zhang, «Carbothermal treated iron oxide nanoparticles with improving magnetic heating efficiency for hyperthermia», *Results in Physics*, vol. 32, ene. 2022, doi: 10.1016/j.rinp.2021.105095.

[57] S. Pakapongpan, Y. Poo-arporn, A. Tuantranont, y R. P. Poo-arporn, «A facile one-pot synthesis of magnetic iron oxide nanoparticles embed N-doped graphene modified magnetic screen printed electrode for electrochemical sensing of chloramphenicol and diethylstilbestrol», *Talanta*, vol. 241, may 2022, doi: 10.1016/j.talanta.2021.123184.

[58] A. Gallo-Cordova *et al.*, «Unravelling an amine-regulated crystallization crossover to prove single/multicore effects on the biomedical and environmental catalytic activity of magnetic iron oxide colloids», *Journal of Colloid and Interface Science*, vol. 608, pp. 1585-1597, feb. 2022, doi: 10.1016/j.jcis.2021.10.111.

[59] A. Gallo-Cordova *et al.*, «Improving degradation of real wastewaters with self-heating magnetic nanocatalysts», *Journal of Cleaner Production*, vol. 308, jul. 2021, doi: 10.1016/j.jclepro.2021.127385.

[60] R. Mithun Prakash *et al.*, «One-step solution auto-combustion process for the rapid synthesis of crystalline phase iron oxide nanoparticles with improved magnetic and photocatalytic properties», *Advanced Powder Technology*, vol. 33, n.º 2, feb. 2022, doi: 10.1016/j.apt.2022.103435.

[61] F. Shahbazi, M. Noghani, y R. Ahmadi, «Effect of synthesis conditions on the morphology, composition and magnetic properties of the iron oxide nanoparticles prepared via electric discharge method», *Journal of Magnetism and Magnetic Materials*, vol. 536, oct. 2021, doi: 10.1016/j.jmmm.2021.168090.

[62] T. Belin, N. Guigue-Millot, T. Caillot, D. Aymes, y J. Niepce, «Influence of grain size, oxygen stoichiometry, and synthesis conditions on the γ-Fe2O3 vacancies ordering and lattice parameters», *Journal of Solid State Chemistry*, vol. 163, n.º 2, pp. 459-465, 2002.

[63] E. Múzquiz-Ramos, V. Guerrero-Chávez, B. Macías-Martínez, C. López-Badillo, y L. García-Cerda, «Synthesis and characterization of maghemite nanoparticles for hyperthermia applications», *Ceramics International*, vol. 41, n.º 1, pp. 397-402, 2015.

[64] H. Shokrollahi, «A review of the magnetic properties, synthesis methods and applications of maghemite», *Journal of Magnetism and Magnetic Materials*, vol. 426, pp. 74-81, 2017.